JGR Earth Surface

RESEARCH ARTICLE
10.1029/2022JF006796

Modeling the Genesis of Sand-Starved Dunes in Steady Currents

Gaetano Porcile[1], Johan H. Damveld[2], Pieter C. Roos[2], Paolo Blondeaux[3], and Marco Colombini[3]

[1]Coastal and Continental Morphodynamics Laboratory, University of Caen Normandy, Caen, France, [2]Water Engineering and Management, University of Twente, Enschede, The Netherlands, [3]Department of Civil, Chemical and Environmental Engineering, University of Genoa, Genoa, Italy

Key Points:

- Our model results indicate that sediment starvation affects fluvial dunes, whose spacing increases as sediment availability decreases
- A quasi-linear and a fully nonlinear model predict larger wavelengths for sediment starved dunes than for their contiguous counterparts
- Modeling outcome conforms with those of previous flume experiments and existing measurements of starved fluvial dunes in the field

Correspondence to:
G. Porcile and J. H. Damveld,
gaetano.porcile@edu.unige.it;
j.h.damveld@utwente.nl

Citation:
Porcile, G., Damveld, J. H., Roos, P. C., Blondeaux, P., & Colombini, M. (2023). Modeling the genesis of sand-starved dunes in steady currents. *Journal of Geophysical Research: Earth Surface*, *128*, e2022JF006796. https://doi.org/10.1029/2022JF006796

Received 14 JUN 2022
Accepted 6 DEC 2022

Author Contributions:
Conceptualization: Gaetano Porcile
Data curation: Gaetano Porcile
Methodology: Gaetano Porcile, Johan H. Damveld, Paolo Blondeaux, Marco Colombini
Software: Johan H. Damveld
Supervision: Pieter C. Roos, Paolo Blondeaux, Marco Colombini
Validation: Gaetano Porcile, Johan H. Damveld
Visualization: Gaetano Porcile, Johan H. Damveld
Writing – original draft: Gaetano Porcile
Writing – review & editing: Gaetano Porcile, Johan H. Damveld, Pieter C. Roos, Paolo Blondeaux, Marco Colombini

Abstract The formation of fluvial dunes is usually studied by investigating the time development of a small amplitude bottom perturbation of a uniform stream and considering that the dunes originate by the growth of the bottom mode characterized by the largest amplification rate under the assumption of an infinite availability of the mobile sediment (linear stability analysis). Here we undertake the stability analysis investigating the formation of sand dunes in steady currents by accounting for the nonlinear effects of sediment starvation on the formative mechanisms of the bedforms and comparing the theoretical results with laboratory experiments, and an application of a fully nonlinear commercial model of finite amplitude dunes, thus enabling an improved understanding of the genesis of starved fluvial dunes. As the growth of the dunes progressively exposes the motionless substratum, both the stability-based and the numerical models predict starved dunes characterized by increasing crest-to-crest distances. The increase of the crest-to-crest distance corresponds to a decrease of the length of individual dunes as well as a growing irregularity in their spacing and morphology. These findings conform with the outcome of physical experiments performed earlier in a laboratory flume and existing measurements of starved fluvial dunes in the field.

Plain Language Summary The genesis of fluvial dunes is a topic of considerable interest to river engineering as dunes are a primary source of flow resistance, regulating water levels and transport processes. The modeling of fluvial dunes is usually performed assuming an infinite availability of the sediment that can be eroded and deposited by the water flow. Field observations and laboratory experiments nevertheless indicate that the supply of sediment affects dune growth and the resulting morphology of the river bed. Here we present a new theoretical model able to reproduce the effects that the lack of sediment has on the growth of dunes and compare it against laboratory experiments, and a numerical commercial model. Our results show that a progressively decrease in sediment supply leads to an increase in dune spacing and a decrease in dune length corresponding to steeper longitudinal profiles. These findings agree with the results of laboratory experiments and existing measurements in the field. As such, this study paves the way to the modeling of fluvial dunes in sediment starved environments and the prediction of their effects on the river flow.

1. Introduction

River beds are seldom flat and those that contain sand generally exhibit a variety of bedforms, ranging from small-scale transverse ripples to large-scale longitudinal alternate bars (Allen, 1968). Indeed, whenever the shear induced by water flowing over a granular surface exceeds the threshold value for sediment motion, sediment particles begin to move and then sediment patterns might appear as a result of the instability of the flat erodible river bed (Seminara, 2010). The flow of water and sediment produces these bedforms, which, in turn, profoundly influence water levels and sediment transport locally affecting mass and momentum transfer. In particular, transverse bedforms typically grow perpendicular to the main direction of the river stream and thus their presence is a primary source of bottom roughness and a major factor in determining water levels (Engelund & Fredsoe, 1982). For practical purposes, the effect that these bedforms have on the hydrodynamics can be modeled as a hydraulic roughness of appropriate size. As such, unraveling the processes underlying their morphology is a subject of great concern to river engineering.

Fluvial dunes are one dimensional bedforms periodic in the longitudinal direction. They exhibit asymmetric profiles with fairly regular crests migrating invariably down-stream (Guy et al., 1966). Their typical crest-to-crest distances scale with the local water depth and their appearance is associated with subcritical flows in the Froude

sense (Colombini, 2004). Because of their significance in formulating depth-discharge relations for river flows and predictor formulas for sediment transport, fluvial dunes received extensive attention from engineers and geomorphologists.

Many field observations and laboratory measurements indicate that sediment patterns commonly observed where the supply of sand is enough to allow the formation of contiguous dunes, differ from those formed where the limited supply of sediment affects the formation of the bedforms. Hereinafter we will refer to the latter conditions as sediment starvation. In this study, sediment starvation is related to a lower limit to the mobile bed of sand that constitutes a hard unerodable substratum. Depending on the given average thickness of the sand layer, the formation of morphologically different bedforms is documented. Contiguous patterns form in the case of a sediment layer thicker than the amplitude of dunes in equilibrium with the local hydrodynamics. When the thickness of the sediment layer equals this threshold value, local sediment starvation is attained and the hard unerodable substratum is exposed in the dune troughs. For smaller values of the sediment layer thickness, widespread sediment starvation affects bedform morphology leading to the formation of starved dunes.

In fluvial environments sediment starvation is common. As channel slopes decrease, rivers typically exhibit abrupt transitions from gravel to sandy bottoms. In these transitional settings, seasonal and perennial gravel-bed streams subject to periods of low flow or discharge waves undergo a transient degradation until the river bed is fully armored (Parker et al., 1982). Then the natural formation of such armored layers inhibits the entrainment of finer sediment from the bed, eventually resulting in sediment starvation. When the armored bed is developed and finer material continues to be supplied to the water flow, starved dunes may appear. Also, recent studies reveal that low-slope bedrock reaches are common in engineered rivers and densely populated deltas (Jafarinik & Viparelli, 2020) and that sandy patterns in these streams are affected by sediment starvation (Jafarinik et al., 2019).

Recent advances in the physical modeling of fluvial starved bedforms revealed the effects of sediment starvation on bedform development. By means of a very simple phenomenological experiment, Venditti et al. (2017) described a definable sequence of starved bedforms emerging in steady currents depending on the supply of sediment. As the sediment supply from upstream increases, a gradual transition occurs starting from longitudinal sand ribbons to three-dimensional barchans that eventually coalesce into amorphous sandy mounds ultimately leading to the generation of two-dimensional transverse dunes (Kleinhans et al., 2002). However, still unclear is how the lack of sediment affects the morphology of the resultant starved dunes. Only a few observations are available (Carling, Golz, et al., 2000; Kleinhans et al., 2002; Venditti et al., 2019) and measurements do not indicate a clear evolution in time. The same difficulty arises when modeling the problem in a flume. The laboratory experiments of Tuijnder et al. (2009) show dune dimensions that progressively decrease as the volume of the finer mobile sediment decreases and the immobile coarser underlayer is exposed. In contrast, the experimental data of Porcile et al. (2020) describe starved dunes attaining longer wavelengths than their contiguous counterparts, for the same values of the hydrodynamic and morphodynamic parameters.

A first theoretical, process-based approach to the study of sand dune formation was proposed by Kennedy (1969), who introduced the idea that fluvial dunes can be the result of a free instability of a uniform steady flow over an alluvial bed. In the following decades, several researchers investigated the formation of dunes and ripples by means of a linear stability analysis (Colombini, 2004; Colombini & Stocchino, 2011; Engelund, 1970; Reynolds, 1976; Richards, 1980). An extensive review of the linear stability analyses of alluvial bed forms can be found in Colombini and Stocchino (2012).

All these theoretical investigations consider an infinite availability of mobile sediment, corresponding to the case in which the mobile sand layer is thick enough to allow the formation of contiguous dunes, and thus they are invalid in the case of sediment starvation. Blondeaux et al. (2016) and Porcile et al. (2017) investigated the effects of sediment starvation on the formation of sea-wave ripples and tidal dunes, respectively. They simulated the formation of small-amplitude starved bedforms in oscillatory currents by means of an idealized model based on a stability analysis. Here a similar theory is applied to steady currents. The analysis can be considered as an extension of the linear stability analysis of Colombini (2004) including the effect of sediment starvation. Our main hypothesis is that when a motionless substratum is exposed by the formation of dunes, the local lack of sand affects the overall sediment transport, and, in turn, the resulting dune morphology. By following the modeling procedure outlined in Blondeaux et al. (2016), this hypothesis is formulated through numerical means. Note that the focus of the paper is on the effects that sediment supply alone has on dune morphology, while the possible changes of flow resistance due to the baring of a rigid bottom are not taken into account.

We apply this model to the formation of laboratory-scale sand dunes by assuming hydrodynamic and sediment transport parameters in line with flume experiments previously performed at the University of Genoa (Porcile et al., 2020). Model results describe starved dunes with an increased crest-to-crest distance and an increasing irregularity in their spacing as their growth progressively exposes the unerodible substratum.

Then, we drop the limiting assumption of the stability analysis which considers small dune amplitudes with respect to the local water depth, and we perform a fully numerical modeling of finite-amplitude starved dunes. We develop an application of the commercial model Delft3D capable of describing the formation of sand dunes in steady currents while accounting for sediment starvation. Analogously to the small-amplitude dune model, the presence of a motionless substratum is included that can lead to sediment starvation depending on initial sediment availability and forcing conditions. The numerical results confirm the findings of the linearized solution, thus suggesting that the lack of sediment available for transport dictates the dimensions of fluvial dunes, potentially affecting the frictional force they exert on the overlying flow.

This paper is organized as follows. Section 2 is devoted to a brief description of the experimental measurements of Porcile et al. (2020) that we use to provide controlled empirical foundations for the development of process-based idealized models of the genesis of sand-starved dunes in steady currents. In Section 3.1 we formulate a stability analysis of sandy beds forced by steady currents considering a limited availability of mobile sediment. In Section 3.2 we introduce a fully numerical model of the formation of finite-amplitude starved dunes. Section 4 presents the results of our modeling exercises. Then, these results are thoroughly compared with previous laboratory measurements and field observations in Section 5. Conclusions are drawn in Section 6.

2. Background: Flume Experiments by Porcile et al. (2020)

Porcile et al. (2020) described experimental measurements of the formation of starved dunes carried out in a laboratory flume at the University of Genoa. These flume experiments were designed to provide further data on the effects of sediment starvation on the formation of fluvial dunes and to compare results of the present numerical investigation with laboratory measurements. Three sets of experiments were performed by fixing all the hydrodynamic and morphodynamic parameters, except the thickness of the layer of sediment initially available for transport. The duration of the experiments was also kept constant. The formation of contiguous and starved dunes was monitored for 30 min. The choice of fixing the same duration of the individual experiments was made to compare morphological configurations obtained at the same stage of the bottom evolution, thus highlighting the effect of supply limitation alone. A time interval equal to 30 min was chosen because at that time dunes were well developed in each experiment and their amplitude development was relatively slow. Note that this does not mean that they were in equilibrium with the forcing flow. Well-sorted sand characterized by a mean grain size $d_s^* = 1.12$ mm was glued on the bottom of the flume, thus creating a rough bed. Before water was pumped through the flume, the same sand was spread on the rough fixed bottom, generating a sand layer with an initial uniform thickness Δ^*, that can be varied per experiment. This setup allowed us to investigate the effects of sediment starvation alone by progressively decreasing the thickness of the initial sand layer (see Porcile et al. (2020) for additional details on the apparatus and experimental procedure).

The bed elevation recorded at the end of the experiments along the centerline of the flume showed that well-defined sand dunes emerged from a uniform sand layer independently on the initial sediment availability (Figure 1). When the emerging bedforms were not high enough to expose the unerodable bottom of the flume, bed profiles of contiguous dunes were observed (Figure 1 top panel). The average wavelengths of these contiguous dunes were approximately the same during all the experiments, showing triangular shapes with gentle stoss sides and steep lee sides. As soon as the growth of the dunes led to the exposure of the flume bottom, regularly spaced transverse dunes were replaced by bump-shaped starved bedforms with steep stoss and lee sides separated by flat troughs (Figure 1 middle and bottom panels).

The average wavelength (i.e., crest-to-crest distance) of starved dunes markedly increased when starting off with a thinner initial sand layer. The bedform wavelength and their spacing were highly correlated. When their spacing increased, their crest-to-crest distance increased as did their irregularities. In contrast, the length of starved dunes (i.e., the distance between the beginning of the stoss face and the end of the lee face of each individual bedform) decreased, corresponding to steeper stoss and lee sides. Moreover, an increasing irregularity in dune spacing associated with a decreasing thickness of the initial sand layer also was observed. In some cases, the strongest

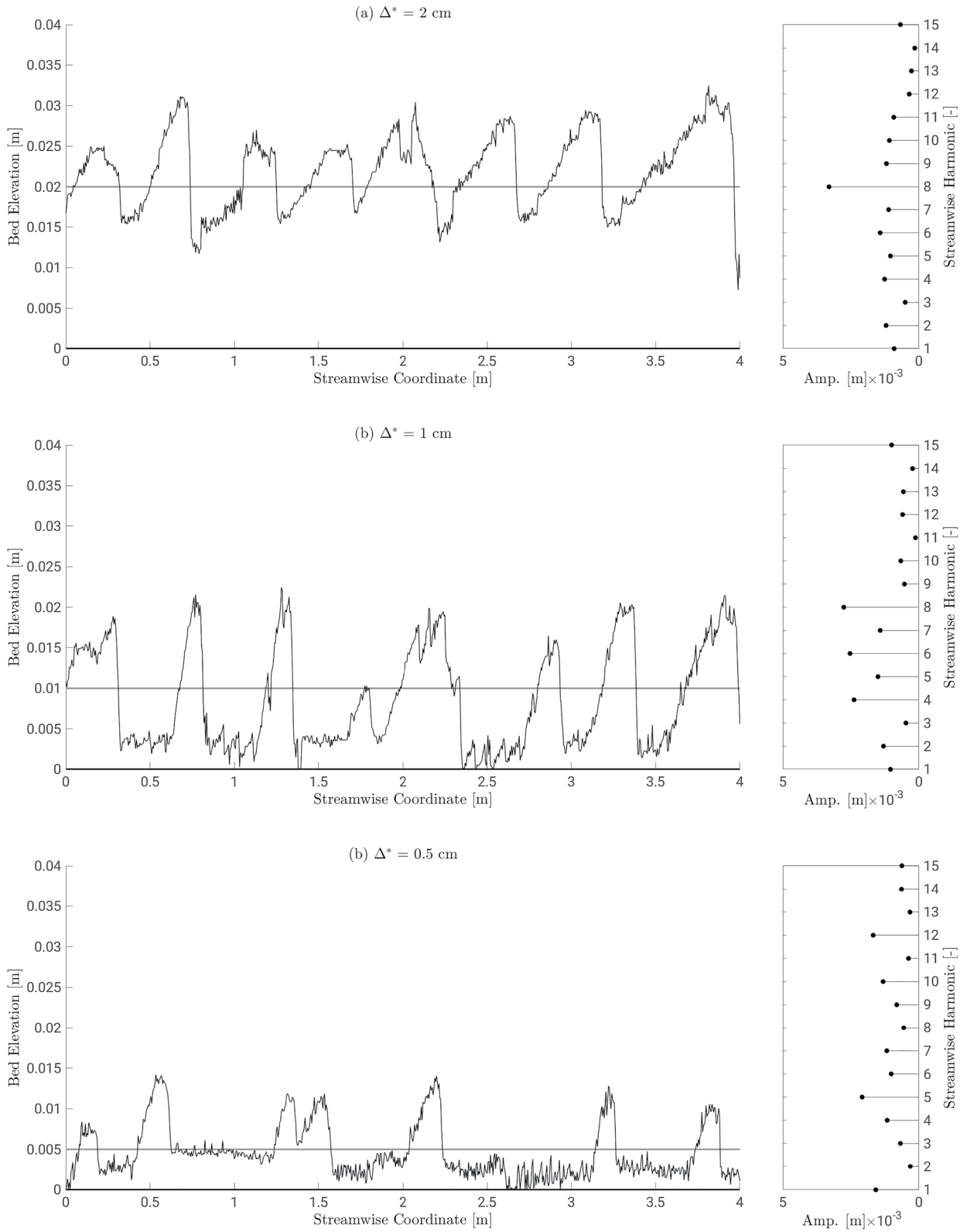

Figure 1. Laboratory measurements of Porcile et al. (2020). Left panels: final bottom configurations measured along the centerline of the flume for decreasing values of the initial uniform thicknesses of the sand layer $\Delta^* = 2$ (top), $\Delta^* = 1$ (middle), and $\Delta^* = 0.5$ cm (bottom). Forcing flow direction is from left to right. Thin black lines represent the bed elevations, thick black lines show the rigid bottom of the flume while thick gray lines show the initial level of the sand layer. Right panels: Spectra of the final bottom configurations. The amplitude of the Fourier components is plotted versus the streamwise harmonic.

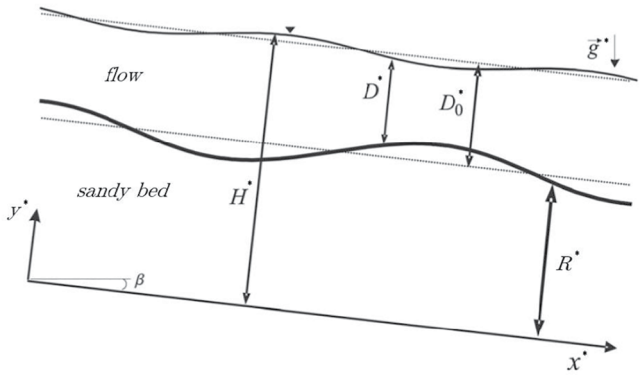

Figure 2. Sketch of the hydrodynamic model showing the sloping streamwise x^*-axis, the almost vertical y^*-axis pointing upwards, the local water depth D^* and the reference level R^*.

sediment starvation resulted in the appearance of three-dimensional barchan dunes. The increasing wavelength of starved bedforms is also shown by the Fourier spectra of the bottom profiles (Figure 1 right panels), which provide a measure of the increasing spacing of starved dunes and allow for a rough estimation of their average wavelength. Streamwise profiles of contiguous dunes were characterized by peak harmonic components corresponding to approximately 0.5 m average wavelength. The spectra of starved dunes show that the peak harmonic component shifts towards lower frequencies as the initial availability of sediment decreases, confirming the marked increase of their wavelength.

3. Methods

Here we describe both the quasi-linear model (Section 3.1), whereby a linear flow model provides the stress field, a predictor relationship computes the associated sediment transport and the Exner equation is integrated numerically including the effect due to sediment starvation, and the fully nonlinear Delft3D model (Section 3.2).

For both models, the flow of an incompressible fluid in a wide straight channel is considered and the Reynolds averaged Navier Stokes (RANS) equations on a vertical plane (2DV) together with the 1D form of the Exner equation are used to describe the hydrodynamics and the bed evolution, respectively.

3.1. Quasi-Linear Model

By adopting the so-called quasi-steady approximation, whereby the flow is assumed to adapt instantaneously to variations of the bed elevation, the solution of the morphodynamic problem can be split in two parts: (a) the solution of the steady flow equations above a fixed periodic bed, which provides the flow response to a given bed perturbation in terms of the stress acting on the bed; (b) the solution of the Exner equation, which provides the evolution of the bed perturbation in terms of propagation and amplification. An algebraic empirical relationship provides the link between these two steps, relating the local value of the net sediment transport to the local value of the stress acting on the bed.

In the quasi-linear model, at any given time, the spatially periodic bed topography is decomposed in a finite number of harmonics. Moreover, the amplitudes of the bed harmonics are assumed to remain small enough for the linear approximation to hold, so that the flow field is expressed as the superposition of the (linear) flow response to each of the bed harmonics. Then, the shear stress distribution at the bed provided by the hydrodynamic module is fed to the morphodynamic module, where the stress field is converted to a sediment discharge distribution. If part of the motionless substratum is exposed, a suitable numerical procedure is employed, which corrects the sediment transport rate to account for the local unavailability of erodible sediment. Finally, the new bed topography is evaluated by means of a numerical integration of the Exner equation.

3.1.1. Hydrodynamics

The formulation of the hydrodynamic module follows closely the one adopted by Colombini (2004) and by Colombini and Stocchino (2005, 2008), which is summarized briefly in the following. The interested reader is referred to the above works for the details of the flow model.

A steady, turbulent free-surface flow is considered in the domain sketched in Figure 2, whereby the streamwise x^*-axis is sloping with slope $S \equiv \tan(\beta)$ and the almost vertical y^*-axis points upwards (hereinafter an asterisk denotes dimensional quantities). The free-surface is represented by the curve $y^* = R^* + D^*$, where D^* is the local water depth and R^* indicates the reference level, that is, the average level at which conventionally the mean logarithmic velocity profile vanishes. This level represents the interface between the fluid flow and the river bed and depends primarily on the bottom roughness.

The triplet composed by the (constant) fluid density ρ^* and by the uniform flow depth D_0^* and shear velocity $u_{\tau 0}^*$ is used for nondimensionalization

$$(x, y) = \frac{(x^*, y^*)}{D_0^*}, \qquad (U, V) = \frac{(U^*, V^*)}{u_{\tau 0}^*}, \qquad P = \frac{P^*}{\rho^* u_{\tau 0}^{*2}}, \qquad T_{i,j} = \frac{T_{i,j}^*}{\rho^* u_{\tau 0}^{*2}}, \tag{1}$$

where P is the ensemble-averaged pressure and (U, V) are the ensemble-averaged velocity components in the x and y directions, respectively. Moreover, T_{ij} are the dimensionless Reynolds stresses

$$\mathbf{T} = \begin{bmatrix} T_{xx} & T_{xy} \\ T_{yx} & T_{yy} \end{bmatrix} = \begin{bmatrix} 2\nu_T \frac{\partial U}{\partial x} & \nu_T \left(\frac{\partial U}{\partial y} + \frac{\partial V}{\partial x} \right) \\ \nu_T \left(\frac{\partial U}{\partial y} + \frac{\partial V}{\partial x} \right) & 2\nu_T \frac{\partial V}{\partial y} \end{bmatrix}, \tag{2}$$

and $\nu_T = \frac{\nu_T^*}{u_{\tau 0}^* D_0^*}$ is the dimensionless turbulent eddy viscosity. Neglecting the viscous stresses, the steady, dimensionless 2DV RANS and continuity equations read

$$U \frac{\partial U}{\partial x} + V \frac{\partial U}{\partial y} = -\frac{\partial P}{\partial x} + \frac{SC^2}{\mathrm{Fr}^2} + \frac{\partial T_{xx}}{\partial x} + \frac{\partial T_{xy}}{\partial y}, \tag{3}$$

$$U \frac{\partial V}{\partial x} + V \frac{\partial V}{\partial y} = -\frac{\partial P}{\partial y} - \frac{C^2}{\mathrm{Fr}^2} + \frac{\partial T_{xy}}{\partial x} + \frac{\partial T_{yy}}{\partial y}, \tag{4}$$

$$\frac{\partial U}{\partial x} + \frac{\partial V}{\partial y} = 0. \tag{5}$$

Two parameters are generated by the nondimensionalization procedure, namely the Froude number $Fr = U_0^*/\sqrt{g^* D_0^*}$ and the conductance coefficient $C = U_0^*/u_{\tau 0}$, where U_0^* is the area velocity of the base uniform flow and g^* is the gravitational acceleration. These two parameters are related to one another by the uniform-flow law, yielding:

$$u_{\tau 0}^* = \frac{U_0^*}{C} = \sqrt{g^* D_0^* S} \qquad \Rightarrow \qquad C = \frac{U_0^*}{u_{\tau 0}^*} \simeq \frac{Fr}{\sqrt{S}}. \tag{6}$$

Furthermore, the coordinate transformation

$$\xi = x, \qquad \eta = \frac{y - R(x)}{D(x)}, \tag{7}$$

is introduced, which maps the flow domain of Figure 2 into a rectangular domain.

The turbulent eddy viscosity ν_T is expressed in terms of an algebraic mixing length L as

$$\nu_T = \frac{1}{D} \frac{\partial U}{\partial \eta} L(\eta)^2, \qquad L(\eta) = \kappa D(\eta + \eta_R)(1 - \eta)^{1/2}, \qquad \eta_R = \frac{2.5 d_s}{30}, \tag{8}$$

where η_R is the roughness height, which is assumed to be proportional to the dimensionless roughness and, ultimately, to the dimensionless sediment diameter d_s.

The problem is then closed by an appropriate set of boundary conditions. In particular, at the reference level $\eta = 0$ the velocity components vanish according to the no-slip condition

$$U = 0, \quad V = 0 \quad \text{at} \quad \eta = 0, \tag{9}$$

whereas at the free surface $\eta = 1$, the kinematic boundary condition reads

$$-U \left(\frac{\partial R}{\partial x} + \frac{\partial D}{\partial x} \right) + V = 0 \quad \text{at} \quad \eta = 1. \tag{10}$$

and the dynamic boundary condition yields

$$T_N = 0, \quad T_T = 0 \quad \text{at} \quad \eta = 1, \tag{11}$$

where T_N and T_T represent the normal and tangential components of the stress acting on a surface at constant η, respectively. Finally, periodic boundary conditions are enforced at the upstream and downstream sides of the domain.

3.1.2. Linearization

Assuming that the height of the dunes is much smaller than the local water depth, the flow field can be evaluated by means of a perturbation approach. As far as the formation of regularly spaced dunes is concerned, it is also possible to assume the periodicity of the bottom geometry. The sandy bed can then be written as superposition of different spatial components which evolve each independently from the others. Of note, with the goal of extending the analysis to starved dunes, the number of spatial components should be large enough to properly describe those transition regions where the exposition of the unerodible substratum occurs. Presently, the following normal-mode representation for the perturbed variables is adopted

$$F(\xi,\eta) = F_0(\eta) + \epsilon F_1(\xi,\eta) = F_0(\eta) + \epsilon f(\eta) e^{i\alpha\xi} + c.c., \tag{12}$$

where ϵ is a small parameter and α denotes the longitudinal dimensionless wavenumber of the generic harmonic component of the perturbation.

Substituting the above splitting formula into the system of Equations 3–5 and boundary conditions Equations 9–11 and collecting terms at the same order of magnitude in ϵ, a set of ordinary differential equations is derived at $\mathcal{O}(\epsilon)$. The resulting two-points boundary value problem is eventually solved by means of a shooting method. In particular, the flow response to a perturbation of the bed of amplitude r can be determined in terms of the shear stress t_{tb} evaluated at the saltation level η_B, which represents the interface between the flowing fluid and the saltation layer, that is, the thin bottom layer were bedload transport takes place (Colombini, 2004). Moreover, the saltation level is assumed parallel to the reference level at a distance equal to the bedload layer thickness

$$\eta_B - \eta_R = l_B d_s = \left\{ 1 + a_B \left(\frac{T_{TR} - T_{TC}}{T_{TC}} \right)^{m_B} \right\} d_s. \tag{13}$$

where T_{TR} and T_{TC} are the shear stress evaluated at the reference level and its critical threshold for incipient motion. The empirical parameters a_B, m_B are set equal to 1.42 and 0.64, respectively (Colombini & Stocchino, 2008).

As expected from a linear, normal-mode analysis, we eventually obtain:

$$t_{tb} = t_t(\eta_B) = r\,\widehat{t}_{tb} \tag{14}$$

where $\widehat{t}_{tb}$ only depends on the wavenumber α and on the flow parameters Fr and C (see Colombini (2004) for the details of the above procedure).

3.1.3. Morphodynamics

In the present formulation, suspended sediment transport is neglected and only bed-load transport is considered, that is, only sliding, rolling, and saltating grain particles are assumed to provide a significant contribution to the sediment transport rate. Such an assumption seems reasonable since sand dunes are more likely to appear in sub-critical flows (Fredsøe, 1974), the bottom shear stress generated by which do not usually produce large suspension of sediment. A common and useful approach to the quantification of bedload transport is to empirically relate the volumetric sediment transport rate per unit width q_S^* with the difference between the bottom shear stress T_{TB}^* and the critical threshold value for incipient motion T_{TC}^*. As already pointed out in the previous section, in the present study the shear stress is evaluated at the saltation level. A large number of empirical relations have been derived using flume data from many laboratory experiments, and these relations share the structure

$$\frac{q_S^*}{\sqrt{(s-1)g^* d_s^{*3}}} = \Phi(\Theta_B, \Theta_C), \tag{15}$$

where $s = \rho_s^*/\rho^*$ is the relative density of the sediment, Φ is the dimensionless bed-load transport rate and Θ_B is the Shields parameter built upon the bed shear stress at level B. More precisely, we have:

$$\Theta_B = \frac{T_{TB}^*}{g^*\rho^*(s-1)d_s^*} = T_{TB}\Theta_{R0}, \qquad \Theta_{R0} = \frac{S}{(s-1)d_s}, \tag{16}$$

where Θ_{R0} is the Shields parameter evaluated at the reference level for the base uniform flow.

Among the commonly adopted bed-load transport predictors is the Fernandez Luque and Van Beek (1976) formula, which reads

$$\Phi = 5.7(\Theta_B - \Theta_C)^{3/2} \quad \text{if} \quad \Theta_B > \Theta_C, \Phi = 0 \quad \text{if} \quad \Theta_B \simeq \Theta_C. \tag{17}$$

This predictor relation is employed as it contains the main physical ingredients controlling the process of sediment transport for values of the Shields parameter close to its threshold value. Furthermore, the bed material tested in the experiments, on which the above relation is based, included different grain sizes ranging from sand to gravel.

Since the problem under consideration accounts for the presence of bottom perturbations, the bed is not flat and the stabilizing effect of gravity, which opposes the uphill motion and favors the downhill motion, is considered by correcting the threshold Shields stress Θ_C (Fredsøe & Deigaard, 1992)

$$\Theta_C = \Theta_{CH}\left[1 - \left(S - \frac{\partial B}{\partial \xi}\right)\frac{1}{\mu_d}\right], \quad \text{with} \quad \Theta_{CH} = 0.038, \tag{18}$$

where Θ_{CH} is the critical Shields value for vanishing slope according to the Fernandez Luque and Van Beek (1976) experimental measurements carried out using sand particles with mean grain size of 0.9 mm and density of 2,640 kg/m^3 which are values very close to our experimental and numerical conditions and μ_d is a dynamic friction coefficient, which is set equal to one half of the Coulomb coefficient μ_c following the recommendations by Fredsøe and Deigaard (1992). Since $\mu_c = \tan(\Psi)$, Ψ being the angle of repose of the sediment and taking into account that, for natural sediments, the angle of repose Ψ ranges between 30° and 50°, the friction coefficient μ_c ranges between 0.58 and 1.2. In this study we employed $\mu_c = 1.0$.

Finally, the development of small-amplitude bottom perturbations can be estimated by means of the sediment continuity equation, which states that the positive (negative) divergence of the sediment transport rate is locally balanced by the decrease (increase) of the bottom elevation

$$\frac{\partial R}{\partial T} = -\frac{\partial \Phi}{\partial \xi}, \qquad T = \frac{t^*\sqrt{(s-1)g^* d_s^{*3}}}{D_0^{*2}(1-p)}, \tag{19}$$

where T is a slow morphodynamic time coordinate.

3.1.4. Linearization

Under the hypothesis of small amplitude bed perturbations, the algebraic relationships Equations 16–18 can be linearized, providing the linear response of the flow to a given bed perturbation in terms of the equilibrium (at capacity) sediment discharge.

In particular, we expand the bedload discharge Φ, the Shields parameter Θ_B and its critical value Θ_C as in Equation 12

$$\Phi(\xi) = \Phi_0 + \epsilon\phi e^{i\alpha\xi} + c.c., \tag{20}$$

$$\Theta_B(\xi) = \Theta_{B0} + \epsilon\theta_b e^{i\alpha\xi} + c.c. = \Theta_{R0}\left[1 - \eta_B + \epsilon t_{tb} e^{i\alpha\xi} + c.c.\right], \tag{21}$$

$$\Theta_C(\xi) = \Theta_{C0} + \epsilon\theta_c e^{i\alpha\xi} + c.c. = \Theta_{CH}\left[1 - \frac{S}{\mu_d} + \epsilon i\alpha\frac{1}{\mu_d} r e^{i\alpha\xi} + c.c.\right]. \tag{22}$$

At order ϵ, we eventually obtain

$$\phi = \left(\frac{\partial \Phi}{\partial \Theta_B}\right)_0 (\theta_b - \theta_c) = \left(\frac{\partial \Phi}{\partial \Theta_B}\right)_0 \left(\Theta_{R0}\hat{t}_{tb} - \Theta_{CH}\frac{i\alpha}{\mu_d}\right) r = \hat{\phi} r \tag{23}$$

where, as for Equation 14, the complex quantity $\hat{\phi}$ only depends on the wavenumber α and on the flow and the sediment parameters for the base state.

Let us now consider the case of infinite availability of sediment or the case in which the lower limit of the mobile sediment layer corresponding to a hard unerodable substratum is deep enough to allow the formation of contiguous dunes without leading to sediment starvation. In these cases, with the additional hypothesis of small amplitude bottom perturbation, the Exner continuity Equation 19 can be linearized. To this end, the reference level R is expanded as

$$R(\xi,T) = R_0 + \epsilon R_1(\xi,T) = R_0 + \epsilon r(T) e^{i\alpha\xi} + c.c. \tag{24}$$

and substituted into Equation 19 to obtain the dispersion relationship

$$\frac{1}{r}\frac{dr}{dT} = -i\alpha\frac{\phi}{r} = -i\alpha\hat{\phi} \;\Rightarrow\; r(T) = e^{-i\alpha\hat{\phi}T} = e^{\Omega T}e^{-i\alpha\omega T}, \tag{25}$$

where $\hat{\phi}$ represents the complex wavespeed of the perturbation and

$$\omega = \mathrm{Re}\left(\hat{\phi}\right), \qquad \Omega = \alpha\mathrm{Im}\left(\hat{\phi}\right), \tag{26}$$

are the celerity and growth rate of the bed perturbation, respectively.

An exponential dependence of the solution on time emerges, as expected in a linear stability analysis. The growth rate is found to be

$$\Omega = \alpha^2\Theta_{R0}\left(\frac{\partial\Phi}{\partial\Theta_B}\right)_0\left(\frac{\mathrm{Im}\left(\hat{t}_{tb}\right)}{\alpha} - \frac{\Theta_{CH}}{\Theta_{R0}\mu_d}\right), \tag{27}$$

which shows how the emergence of small-amplitude dunes is related to a balance between the destabilizing effect due to the steady current, represented by the shear stress at the bed-load level, and the stabilizing effect due to the gravity, represented by the dynamic friction coefficient. Thus the study of the dispersion relationship allows growing modes with positive growth rate to be identified in the parameter space and, among those, the fastest growing one. Finally, an estimate of the wavelength of the emerging dunes can be predicted by assuming that the most unstable mode prevails on the others during the short-term morphodynamic evolution of the sandy bed.

3.1.5. Modification to Account for Sediment Starvation

When a motionless substratum is exposed by the formation of dunes, the lack of sand affects sediment transport, and, in turn, the pattern morphology. The exposure of the motionless substratum locally prevents the entrainment of sand, leading to sediment starvation. The sediment transport formula Equation 17 quantifying the bed-load sediment transport cannot be applied in the case of sediment starvation unless a suitable numerical procedure is introduced capable of taking into account for the local lack of mobile sediment.

Where sand is available, the sediment transport depends only on the bed shear stress. If the shear decreases (increases) in the flow direction, the sediment transport rate can be predicted by the predictor formula and some deposition (erosion) occurs according to the continuity of the sediment phase. In contrast, where a motionless substratum is locally exposed, the amount of sediment in motion might be smaller than the local transport capacity. In particular, the value of the sediment transport rate $\Phi(x^*)$ depends not only on the value of the shear stress $\Theta_B(x^*)$ but also on its spatial derivative. On one hand, if the shear stress increases in the direction of the flow, the sediment transport rate remains constant since the flow cannot entrain additional mobile sediment because it is not available. On the other hand, if the shear stress decreases in the direction of the flow, two different scenarios are possible depending on the upstream value of the sediment transport rate. If the upstream value of the sediment transport rate is smaller than the local value predicted by the predictor formula $\Phi_P(x^*)$ the local sediment transport rate should be assumed equal to its upstream value. This situation can occur due to the upstream exposure of the motionless substratum. Otherwise, the sediment transport rate can be predicted by the predictor formula and some deposition of sediment over the exposed substratum should occur.

$$\left.\frac{d\Phi}{dx^*}\right|_+ = 0 \quad \text{if} \quad \left.\frac{d\Theta_B}{dx^*}\right|_{x^*} > 0, \tag{28}$$

$$\left.\frac{d\Phi}{dx^*}\right|_+ = 0 \quad \text{if} \quad \left.\frac{\Theta_B}{dx^*}\right|_{x^*} < 0 \quad \text{and} \quad \Phi(x^*) < \Phi_P(x^*), \tag{29}$$

$$\Phi(x^*) = \Phi_P(x^*) \quad \text{if} \quad \left.\frac{\Theta_B}{dx^*}\right|_{x^*} < 0 \quad \text{and} \quad \Phi(x^*) > \Phi_P(x^*). \tag{30}$$

These simple rules Equations 28–30 introduce strong nonlinearities and the time development of the bottom configuration can be obtained only by numerical means. The present model integrates in time and space the dimensionless sediment continuity equation. The time advancement of Equation 19 is solved by means of a Runge-Kutta second order approach, while the spatial derivatives are replaced by their second order finite difference approximations. A computational domain of length L_d^* along the horizontal axis x^* is considered and periodic boundary conditions are applied at its ends. The dimensionless length of the computational domain $L_d = L_d^*/D_0^*$ and the thickness of the initial sand layer $\Delta = \Delta^*/D_0^*$ are free geometrical parameters. The value of L_d should be large enough to assume its influence on the time development of the bottom configuration to be negligible and to properly represent the formation of the fastest growing mode predicted by the linear stability analysis. Because the time development of the entire range of unstable modes has to be described with sufficient accuracy, the spatial discretization should be accurate enough to represent the smaller wavelength of the unstable modes predicted by the linear stability analysis with an appropriate number of computational points.

In the transition regions between the motionless substratum and the erodible bed, small-scale spurious oscillations arise as a result of the Gibbs' effect associated with the discontinuity in the bed slope. In the numerical time-stepping procedure, the model forces the bed elevation to never drop below the level of the substratum by applying a filtering procedure that removes the small-scale spurious oscillations. The results of preliminary simulations repeated halving the grid size, time step, and domain length indicate that the chosen numerical setup does not affect the time development of the bottom configuration. Note that the bed roughness does not change when the hard unerodible substratum is exposed. This choice is made to account for discontinuity in the sediment supply only and thus focusing on nonlinearities due to sediment starvation. Also, the assumption of a uniform bed roughness is in line with previous numerical investigations (Blondeaux et al., 2016; Porcile et al., 2017) and the experiments of Porcile et al. (2020) that were carried out by glueing a small layer of the mobile sediments on the hard unerodible flume bottom.

3.2. Fully Nonlinear Model

3.2.1. General Model Description

The finite-amplitude evolution of fluvial dunes in sediment scarce environments is modeled by means of the numerical shallow water model Delft3D (Lesser et al., 2004). Analogous to the small-amplitude model, the hydrodynamic equations (here in terms of vertical σ-coordinates) consist of the 2DV Navier Stokes equations, a continuity equation and a turbulence closure model, supplemented by appropriate boundary conditions. In contrast to the quasi-linear model, turbulence is modeled by means of the $k_T - \epsilon_T$ turbulence model. Both the bed load and the suspended load are included in the model, and bed evolution is computed by the Exner equation. For an overview of the relevant 2DV model equations, see for example, Damveld et al. (2020).

3.2.2. Model Domain, Boundary Conditions, and Parameter Choices

The horizontal length of the domain is 60 m long and has a uniform grid spacing of 2.5 cm. In the vertical direction the grid consists of 30 σ-layers, with a small thickness (0.25% of the local water depth D^*) near the bed, gradually increasing in the upward direction. At the upstream boundary a logarithmic velocity profile with a constant discharge of 0.03 m^3/s is specified, whereas at the downstream boundary the water level is kept constant throughout the simulations at a level of 12 cm. These values lead to a Froude number Fr = 0.51, similar to those characterizing the flume experiments. The vanishing of the stress tensor was imposed at the free surface. The area of interest is situated in the second half of the domain to ensure that possible upstream boundary disturbances do not migrate into the domain and influence the results. The hydrodynamic time step is set equal to 0.15 s and a spin-up time of 10 min is made during which no bed level changes are allowed. Finally, the roughness of the bed is specified through a roughness length z_0 of 1 mm, which is equal to the sediment diameter. Note that the bed roughness does not change when the bare substrate is exposed, which is in fact in line with the assumption made in the formulation of the quasi-linear model and the experimental setup, where the sediment was glued to the bottom of the flume (Porcile et al., 2020).

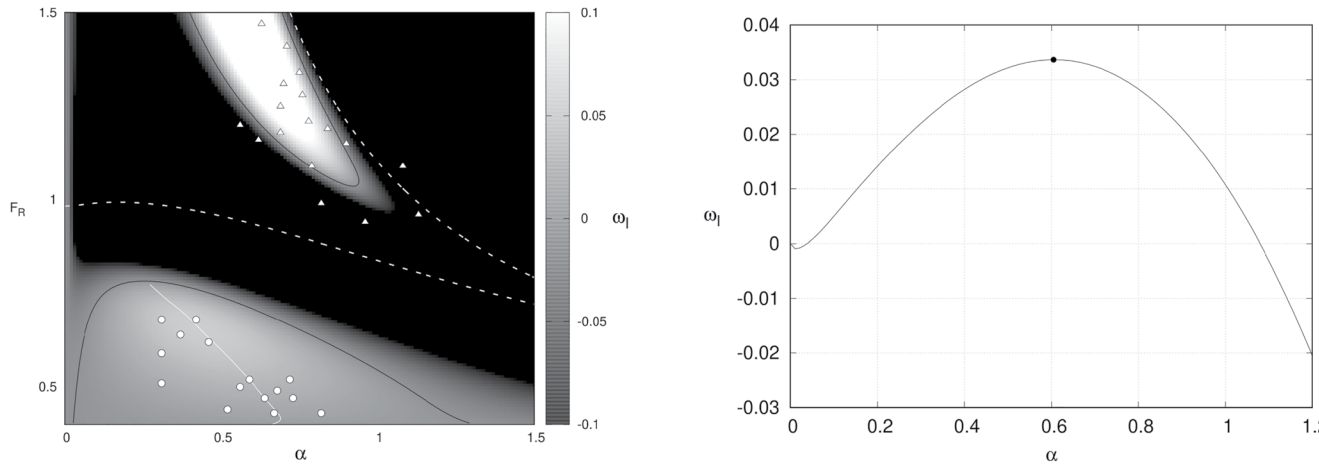

Figure 3. Results of the quasi-linear model in the case of an unlimited sediment supply. Left panel: growth rate plotted in shades of gray for a value of the conductance coefficient $C = 15$. Thick black lines represent the curves of vanishing growth rate, dashed white lines represent the curves of vanishing celerity, white line represent fastest growing modes. The marks indicate the experimental measurements of Guy et al. (1966): circles, dunes; triangles, antidunes. Right panel: growth curve for a value of the Froude number Fr = 0.5 whose maximum identifies the fastest growing mode.

4. Results

Generally, comparing theoretical results of stability analyses with laboratory measurements is difficult. Because the flume width is usually of the same order of the flow depth, the side walls affect the bottom shear stress. If the bottom is rougher than the side walls, as in the experiments by Porcile et al. (2020), the distribution of the shear along the wetted perimeter of the channel is nonuniform. We thus evaluated an equivalent, uniform open-channel flow characterizing the flume experiments by means of the side-wall correction of Vanoni and Brooks (1957), which allows for a proper comparison of our theoretical model results with the laboratory measurements.

4.1. Quasi-Linear Model Results

The investigation of the dispersion relationship Equation 24 allows possible instability regions to be isolated in the parameter space. Among the free parameters of the stability-based model, there are the unperturbed flow depth D_0^* and the uniform mean grain size of the sediment d_s^*, which determine the conductance coefficient characterizing the unperturbed steady stream. In order to compare the laboratory observations with the average wavelength of small-amplitude contiguous dunes predicted by the stability analysis, the value of the mean grain size was set equal to that of the well-sorted sediment used in the experiments. The unperturbed mean water depth was set equal to the uniform depth of the wide open channel flow evaluated by the side-wall correction. Then, the values of the conductance coefficient and the Froude number can be easily evaluated for the unperturbed flow. It follows $C = 15, Fr = 0.5$.

Varying the Froude number, it is possible to compute the growth rate ω_I as well as the value of ω_R which determines the perturbation celerity as function of the dimensionless wavenumber α (see Figure 3). Positive values of the growth rate represent the growth of small-amplitude perturbations, thus indicating instability. On the other hand, the value of ω_R determines the celerity of the perturbations, positive (negative) values indicating downstream (upstream) migration. In left panel of Figure 3 the broken white lines represent vanishing values of the migration rate. Below the lower broken line the celerity of the growing modes is positive (i.e., downstream migration, dunes). The growing modes lying above this line has negative celerity (i.e., upstream migration, antidunes). The good agreement between the identified regions of instability and the experimental data set of Guy et al. (1966) later "side-wall corrected" by Colombini (2004) prove the reliability of the stability analysis.

From the left panel of Figure 3, it is possible to extrapolate the growth curve shown in the right panel of Figure 3 by considering the value of the Froude number equal to 0.5. Hence, the fastest growing mode can be selected among the range of the predicted perturbations. Assuming that this mode prevails during the short-term morphodynamic evolution of the sandy bed, the wavelength of the small-amplitude dunes can be predicted. For the chosen set of parameters the stability analysis predicts the appearance of bottom perturbations characterized by a

wavenumber $\alpha = 0.6$, which corresponds to a value of the dimensional wavelength slightly smaller than $\lambda^* = 1$ m. This value is similar to the wavelengths of the contiguous dunes observed during the experiments, though an overestimation is present.

To test whether the model can provide a reliable description of the genesis of small-amplitude starved dunes as observed during the flume experiments, a series of simulations is performed computing the time development of an initial random bottom waviness forced by a uniform steady current by fixing the hydrodynamic and morphodynamic parameters and varying only the supply of sediment. Analogously to the experimental investigation, the sediment supply is decreased by decreasing the thickness Δ of the initial sand layer through which dunes can develop. Figure 4 shows the bottom configurations at the beginning (gray lines) and at the end (black lines) of each numerical simulation. The values of the Froude number and the conductance coefficient are kept constant during all the numerical simulations and equal to those of the experiments evaluated by means of the side-wall correction. The dimensionless length L_d of the computational domain is equal to 100 and the dimensionless thickness of the initial sand layer is progressively decreased starting from $\Delta = 0.2$ down to $\Delta = 0.05$. Because the experiments are characterized by a dimensional mean water depth $D_0^* = 0.1$ m, the value of Δ^* ranges from 2 to 0.5 cm and the dimensional length of the computational domain is about 10 m. Each numerical simulation is made considering a dimensionless simulation time that is of the same order of magnitude as that of the experiment duration. After 30 min, the model predicts well developed dunes analogously to the laboratory experiments. The quasi-linear model however predicts an exponential growth of the bedforms in the case of sediment abundance, which is different from the slow amplitude development observed in all experiments. Note that this means that the formation stages replicated by the quasi-linear model are not in equilibrium with the forcing flow.

At the beginning of the first simulation (Figure 4a) the bottom is characterized by a random perturbation of small amplitude. Then, the computed bottom profile shows a rapid decay of the perturbation components characterized by very small wavelengths and only the unstable modes predicted by the stability analysis survive. Then, for long time, the growth of the fastest growing mode gives rise to periodic bedforms (dunes). For $\Delta = 0.2$, the appearance of the bottom forms does not bare the motionless substratum and at the end of the simulation, 10 clearly defined dunes can be easily identified through the computational domain with an average dimensional wavelength equal to 10 (Figure 4a). Different results are obtained in the second and third simulations (see Figures 4b and 4c). These results correspond to a dimensionless initial sand layer thickness equal to 0.1 and 0.05, respectively. Progressively decreasing the amount of the sediment available for transport, the motionless substratum is exposed by the growth of the dunes, leading to sediment starvation. Starved dunes show increasing wavelengths as the degree of sediment starvation increases. This increase in dune wavelength corresponds to a decrease of the size of individual bedforms and the increasing irregularity of their profile.

The panels on the right-hand side of Figure 4 show one-dimensional spectra of the final bottom profiles computed by the stability-based model. The modulus of the complex amplitude of each harmonic component of the Fourier transform of the bottom elevation is presented. These spectra reveal whether a dominant wavelength can be identified or whether the bottom configuration is the result of a superposition of many different components. By comparing the harmonic content of each computed bed profile, it is seen that the peak harmonic component shifts toward lower frequencies as the thickness of the initial sand layer decreases.

4.2. Fully Nonlinear Model Results

Next, we repeat our numerical experiments with the finite-amplitude model Delft3D. Again, the only parameter which is varied is the initial thickness of the movable layer of sediments. Figure 5 (left-hand panels) show the initial and final bottom configurations of the simulations. For the sediment abundant case (Figure 5a), asymmetrically shaped dunes develop, with an average crest-to-crest distance slightly larger than $\lambda^* = 1$ m. Similar to the quasi-linear model result, this value is close to the value observed during the experiments. Figures 5b and 5c show a decreasing number of dunes as a result of the decreasing sediment availability. In contrast to the quasi-linear model result, the wave height and spacing of the patterns become more regular over time, especially in the sediment scarce case. This change in form is a good indication that the bottom configuration is close to its equilibrium state after 30 min, analogously to the laboratory experiments. Another effect which can be observed toward the end of the simulations is the asymmetry of the (isolated) bedforms, which are characterized by a shorter lee side.

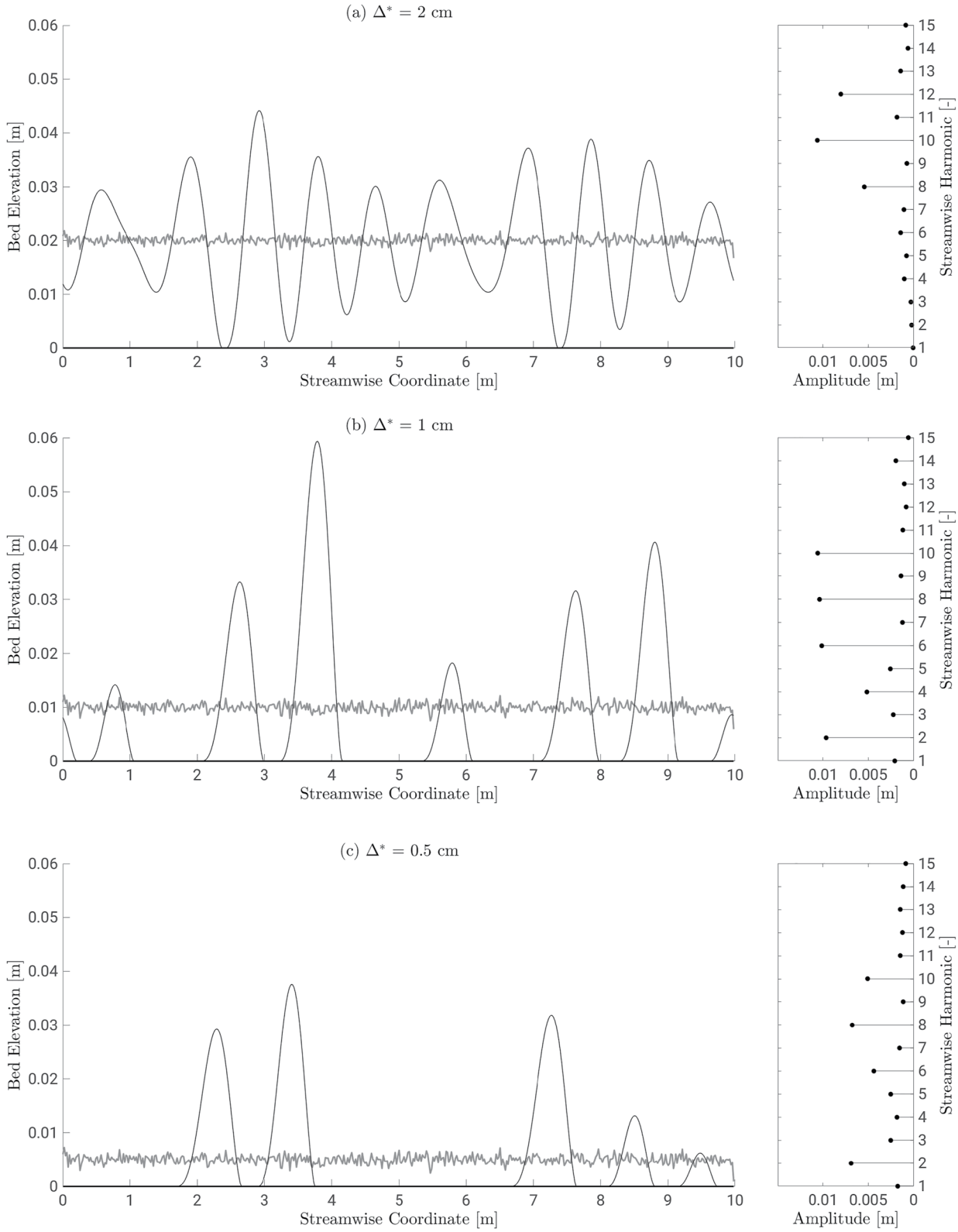

Figure 4. Results of the quasi-linear model in the case of a limited sediment supply. Left panels show the time development of an initial random bottom waviness for dimensionless parameters $C = 15$ and $\mathrm{Fr} = 0.5$ in line with the laboratory experiments of Porcile et al. (2020) and a simulated time-window which is the same as those of their experiments. From (a) top panel to (c) bottom panel, sediment starvation is enforced by decreasing the initial uniform thickness of the sand layer. Thin black lines represent the final bottom configurations, thick black lines show the rigid flume bottom while thin gray lines are the initial random waviness. Right panels show the spectra of the final bottom configurations. The amplitude of the Fourier components is plotted versus the streamwise harmonic.

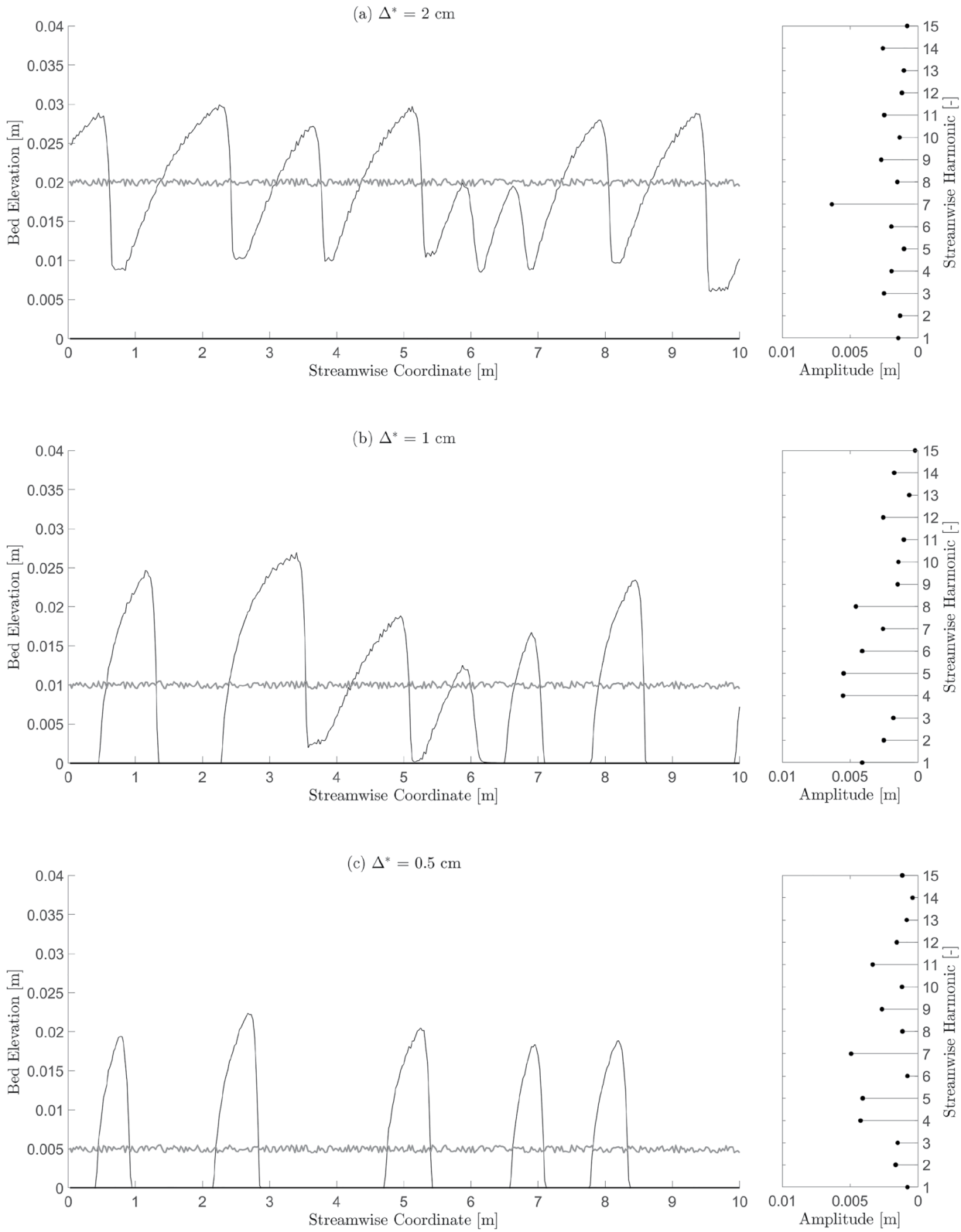

Figure 5. Results of the fully nonlinear model in the case of a limited sediment supply. Left panels show the time development of an initial random bottom waviness considering a simulated time-window which is the same as that of the laboratory experiments of Porcile et al. (2020). From (a) top panel to (c) bottom panel, sediment starvation is enforced by decreasing the initial uniform thickness of the sand layer. Thin black lines represent the final bottom configurations, thick black lines show the rigid flume bottom, while thin gray lines are the initial random waviness. Right panels show the spectra of the final bottom configurations. The amplitude of the Fourier components is plotted versus the streamwise harmonic.

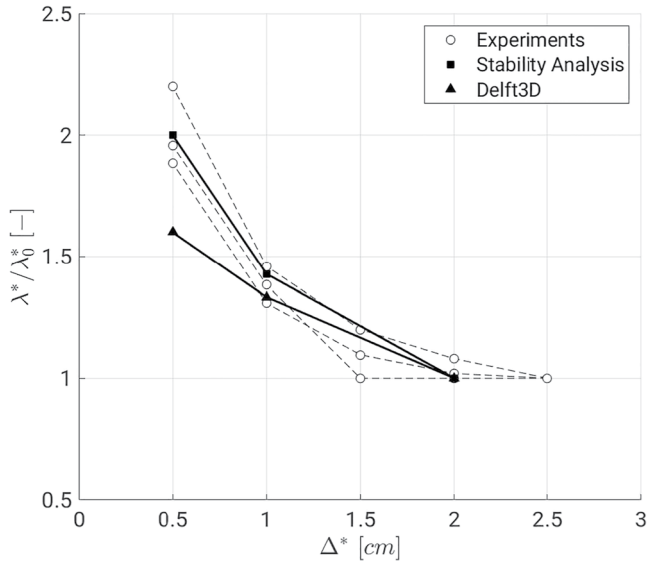

Figure 6. Comparisons of modeling outcomes with experimental measurements of starved dunes. Values of starved dune crest-to-crest distances are normalized by the wavelength of contiguous dunes observed for the same hydrodynamic and morphodynamic parameters and then plotted versus the thickness Δ* of the sand layer initially available for transport.

Similar to the results of the quasi-linear model, the right-hand panels of Figure 5 show the modulus of the Fourier components. Also in this case, it can be observed that the peak shifts toward the lower wavenumbers as the thickness of the mobile sediments decreases. However, this observation is less apparent than in the former case. Due to asymmetrical shape of the morphological patterns, the spectrum of the signal becomes broader and no particular peak stands out.

5. Discussion

The results of the idealized process-based models described in the previous sections agree with the experimental findings of Porcile et al. (2020). Particularly, the models reproduce the same observed effects of sediment starvation on the genesis of sand dunes in steady currents when an uneroda-ble substratum is exposed by the growth of the bedforms. Both the stability analysis based on the numerical simulation of small amplitude perturbations of the bottom configuration and the fully nonlinear commercial model able to simulate the time development of finite amplitude bedforms predict an increasing crest-to-crest distance of sediment starved dunes and a reduction of their individual size as their growth progressively exposes the motion-less substratum, with increasing irregularity of their morphology and spac-ing. Despite the overestimation of dune wavelength obtained by using these two different approaches, both models are able to reproduce the increasing starved dune spacing as observed in the laboratory (Figure 6).

The key findings of our modeling study also agree with existing field measurements of starved fluvial dunes. Kleinhans et al. (2002) described the observations and measurements of several type of bedforms in the gravel-bed river Allier (Moulis, France) over a period of low flow during which the river bed was fully armored. Sand wave fields of fine sand ($d_s \simeq 0 \div 5$ mm), the area of which ranges from few to few hundreds of squared meters, were found to migrate over the armor layer (85% gravel, $d_s \simeq 18$ mm) as a result of bank erosion and detachment of sand from meander pools. These sand waves provided a spatially varying supply of mobile sediment for the formation of bedforms in equal hydrodynamic conditions and sediment parameters. Regularly spaced transverse dunes appeared in the inner part of these sand deposits, where the thickness of the sand coverage attains its maximum value. Then, these bedforms gradually changed in both the upstream and the downstream directions resulting into amorphous bedforms with more sinuous crests. At the front and rear edge of each sand wave field, the armor layer was fully exposed and amorphous dunes concurrently with sand ribbons were observed. Analo-gously to our model results, the field observations of Kleinhans et al. (2002) suggest that the main factor in deter-mining the geometric characteristics of the emerging bedforms is the thickness of the layer of sediment available for transport. The gradual transition from regular contiguous dunes to irregular starved dunes is the same as that observed in the present study.

Similar patterns were observed by Carling, Golz, et al. (2000) and Carling, Williams, et al. (2000) in a supply limited reach of the river Rhine (Mainz, Germany). Carling, Williams, et al. (2000) report the presence of well sorted medium sand ($d_s \simeq 0.9$ mm) in the form of different morphological patterns migrating over gravel lags mainly composed of pebbles and cobbles ($d_s \simeq 10$ mm). Two distinct populations of bedforms were identified: two-dimensional small dunes ($\lambda \simeq 1 \div 5$ m) with relatively straight crest, which were roughly transverse to the primary flow direction, and three-dimensional isolated dunes ($\lambda \simeq 20 \div 50$ m) with either amorphous or barch-anoid planforms. Carling, Williams, et al. (2000) described in detail two large isolated bedforms superimposed by smaller dunes. Despite Carling, Golz, et al. (2000) noted that in many cases the term starved dune might be a misnomer as it is not always clear that there is a shortage of sediment, the size and the planform of isolated dunes and the change in geometry of the smaller bedforms which migrate over the gravel lags preceding isolated dunes and then over the parent bedform seem to confirm that these populations of dunes are affected by sediment starvation. In particular, the smaller dunes moving over the immobile gravel layer show an average wavelength approximately equal to 2 m and were found to decrease in wavelength ($\lambda \leq 1$ m) while migrating over the stoss side of the larger bedforms. Further downstream they appear to have generally grown in dimensions ($\lambda \geq 2$ m)

across the gentle stoss side of the parent dune up to the crestal region, where their transition to upper-stage plane bed was observed. Proceeding further downstream, the smaller dunes often reformed increasing in wavelength and migrating over the intervening gravel lags. All that being said, these field observations seem to indicate that sediment starvation manifests itself by forming static isolated large dunes as well as by affecting the dimensions of migrating small dunes as a contiguous dune field is replaced by their starved counterparts and this is likely due to the exposure of the immobile gravel layer in their troughs. Particularly, the decreased spacing of the small dunes as they migrate from the gravel lags up to the gentle stoss side of isolated barchan dunes is consistent with our model results. As such, our modeling exercise identifies a potential process controlling the development of the observed dunes. Carling, Golz, et al. (2000) noted also that the exposed hard ground in the dune troughs have greater bed roughness and thus modulate turbulence in comparison with contiguous dunes. This turbulence modification might explain the changes in dune form rather than just the wavelengths, potentially affecting the steepness of stoss and lee sides of the bedforms and their three-dimensional planforms.

Other flume experiments designed to study the effects of sediment starvation on dune growth have led to contradictory results. The experiments of Kleinhans et al. (2002) and Venditti et al. (2019) identified a sequence of emerging bedforms in steady currents and the profile of these bedforms was observed to depend on the sediment available for transport. Differently with the experiments we used for our model validation, they provided sediment from upstream, observing the gradual growth of different kind of bedforms. As the sediment supply increased, Kleinhans et al. (2002) found a transition from sand ribbons to irregular sandy mounds and finally two-dimensional transverse dunes. Despite a clear indication on the dimensions of starved dunes with respect to contiguous dunes was not provided, their findings seem qualitatively in agreement with our modeling results. A clear indication that starved dunes have reduced amplitudes and lengths than contiguous dunes not affected by sediment starvation is provided by the experimental measurements of Jafarinik et al. (2019), who measured dune profiles upstream and downstream of an alluvial-bedrock transition.

Similarly, the experiments of Tuijnder et al. (2009) show dune geometries that progressively decrease in size as the availability of mobile sediment decreases and the immobile coarser underlayer is bared by the growth of the dunes. However, they also observed a decreasing wavelength of starved dunes with respect to that of contiguous dunes. Among the several possible explanations to the contradiction between their observations and our results (see Porcile et al. (2020) for an extensive discussion), we believe the difference in the sediment and the associated skin roughness to be crucial. Tuijnder et al. (2009) employed two different grain sizes for the immobile substrate and the mobile layer. The coarser grain size of the substrate was selected to be immobile under the action of the forcing flow. As a consequence, the exposition of the substrate led not only to sediment starvation, but also to a discontinuity in skin bottom roughness. Conversely, our numerical models and the experiments used for their validation assume a substrate roughness which is the same as the skin roughness representing the one single grain size available for transport. An extension of the present modeling by introducing a non-uniform bottom roughness depending on the exposure of the hard unerodable substratum will likely shed light on the roughness control on starved dune formation. Indeed, as Carling, Golz, et al. (2000) pointed out, the exposure of the rough immobile gravel surface in the troughs must affect turbulence generation and represent a major control on starved dune morphology rather than just their wavelengths. However, both models used in this study would require additional developments to include the effects of nonlinearities due to discontinuities in the bottom roughness.

Furthermore, a striking difference between the quasi-linear approach and the fully nonlinear one is the predicted dune shape. It can be seen that the quasi-linear model predicts purely sinusoidal shapes, whereas the fully nonlinear model predicts non-sinusoidal, asymmetric shapes. Comparing this bottom profile with the triangular-shaped dunes observed in the laboratory experiments, this clearly confirms the general idea that strong nonlinearities imply asymmetric dunes.

Less information is available in the literature on the effect that sediment starvation has on the migration of bedforms. The experimental measurements reproduced by our modeling results cannot reveal useful information on starved dunes migration as they were conducted without recirculation of the sediment and thus limited in time (the experiments lasted only 30 min). Thus, future experimental and modeling studies are required to properly investigate the effects that the lack of mobile sediment has on bedform migration.

Finally, in order to place this work within a broader field of research, the presented 2DV hydrodynamic models could be straightforwardly extended in the third direction. There is a body of work that shows that eolian dune size and spacing is the result of finite-amplitude interactions and how these interactions can form isolated

barchans in the desert (Hersen et al., 2004; Khosronejad & Sotiropoulos, 2017; Worman et al., 2013). An extension of the quasi-linear and fully nonlinear models to account for three-dimensional effects could be used for discussing subaqueous barchan dunes as a prominent example of dunes in a sediment-limited environment, rather than necessarily reflecting only finite-amplitude interactions. For instance, the fully nonlinear Delft3D model is currently also used to study sediment starvation in tidal sand waves (Damveld et al., 2021). Hopefully, the flow module of the models could also be extended to study the atmospheric boundary layer making the present models able to investigate the effects of sediment starvation on the morphology of eolian sandy patterns.

6. Conclusions

In this study two different process-based modeling techniques are applied to investigate the genesis of fluvial dunes in case of sediment starvation. Previous laboratory experiments of Porcile et al. (2020) are used to provide controlled empirical foundations for the development of process-based idealized models able to reproduce the effects that sediment starvation has on the growth of these bedforms. An hypothesis is formulated in light of the experimental measurements which states that the lack of sand affects sediment transport and, in turn, bedform pattern, when a motionless substratum is exposed by the formation of fluvial dunes. Then, this hypothesis is tested by means of numerical simulations in the framework of the stability analysis of sandy bottoms forced by steady currents as well as the fully numerical modeling of the time development of the bottom perturbations.

Generally, the laboratory measurements indicate that the exposition of the rigid bottom strongly affects the characteristics of the emerging dunes, whose spacing increases and becomes more irregular with a decreasing initial sediment availability. In line with these experimental findings, the results of the stability-based model describe starved dunes with longer wavelengths and shorter lengths than those of contiguous dunes, for the same values of hydrodynamic and morphodynamic parameters. Finally, a similar modeling outcome is obtained by the finite-amplitude model. Differently from the stability analysis, this fully nonlinear model is able to reproduce final bottom configurations whose profile is even closer to that observed during laboratory experiments, as it accounts for nonlinear effects other than sediment starvation. Predicted longitudinal profiles of starved dunes have steeper stoss and lee sides, corresponding to shorter bedform size. Thus, in sediment starved environments, the crest-to-crest distance of starved dunes can increase whilst the length of the individual bedforms shorten as the bare trough lengths increase.

The comparisons between laboratory experiments and numerical model results investigating the morphodynamics of river reaches with exposed bedrock surfaces show that bedload transport models derived for alluvial systems reasonably predict equilibrium sediment transport rates and bed surface size distributions in bedrock reaches if the presence of exposed bedrock is accounted for in terms of alluvial cover fraction (Jafarinik & Viparelli, 2020). Our modeling exercise demonstrates that numerical models designed to study alluvial systems can also predict the morphological evolution of starved bedforms if the presence of exposed bedrock is considered. As such, this study paves the way to the modeling of field-scale starved dunes and to potentially deal with the long-term dynamics of these patterns to describe their equilibrium geometry and migration. An extension of our modeling exercise would allow to include further nonlinear mechanisms that have been neglected so far, such as those associated with gravity, bottom roughness, sediment sorting, and three-dimensional flow and sediment transport.

Data Availability Statement

Data sets for this research are included in the following paper (and its supplementary information files): Porcile et al. (2020).

Acknowledgments
The authors are grateful for the feedback received from Paul Carling, two anonymous reviewers, the Associated Editor, and the Editor on an earlier version of this manuscript. The second author acknowledges the support by the Dutch Research Council Science (NWO) of the Footprint project, Grant NWA.1236.18.003.

References

Allen, J. (1968). The nature and origin of bed-form hierarchies. *Sedimentology*, *10*(3), 161–182. https://doi.org/10.1111/j.1365-3091.1968.tb01110.x

Blondeaux, P., Vittori, G., & Mazzuoli, M. (2016). Pattern formation in a thin layer of sediment. *Marine Geology*, *376*, 39–50. https://doi.org/10.1016/j.margeo.2016.03.011

Carling, P., Golz, E., Orr, H., & Radecki-Pawlik, A. (2000). The morphodynamics of fluvial sand dunes in the River Rhine, near Mainz, Germany. I. Sedimentology and morphology. *Sedimentology*, *47*(1), 227–252. https://doi.org/10.1046/j.1365-3091.2000.00290.x

Carling, P., Williams, J., Golz, E., & Kelsey, A. (2000). The morphodynamics of fluvial sand dunes in the River Rhine, near Mainz, Germany. II. Hydrodynamics and sediment transport. *Sedimentology*, *47*(1), 253–278. https://doi.org/10.1046/j.1365-3091.2000.00291.x

Colombini, M. (2004). Revisiting the linear theory of sand dune formation. *Journal of Fluid Mechanics*, *502*(1–16), 1–16. https://doi.org/10.1017/s0022112003007201

Colombini, M., & Stocchino, A. (2005). Coupling or decoupling bed and flow dynamics: fast and slow sediment waves at high Froude numbers. *Physics of Fluids*, *17*(3), 036602. https://doi.org/10.1063/1.1848731

Colombini, M., & Stocchino, A. (2008). Finite-amplitude river dunes. *Journal of Fluid Mechanics*, *611*, 283–306. https://doi.org/10.1017/s0022112008002814

Colombini, M., & Stocchino, A. (2011). Ripple and dune formation in rivers. *Journal of Fluid Mechanics*, *673*, 121–131. https://doi.org/10.1017/s0022112011000048

Colombini, M., & Stocchino, A. (2012). Three-dimensional river bed forms. *Journal of Fluid Mechanics*, *695*, 63–80. https://doi.org/10.1017/jfm.2011.556

Damveld, J. H., Borsje, B. W., Roos, P. C., & Hulscher, S. J. M. H. (2020). Horizontal and vertical sediment sorting in tidal sand waves: Modeling the finite-amplitude stage. *Journal of Geophysical Research: Earth Surface*, *125*(10), e2019JF005430. https://doi.org/10.1029/2019JF005430

Damveld, J. H., Porcile, G., Blondeaux, P., & Roos, P. C. (2021). Nonlinear dynamics of sand waves in sediment scarce environments. In *EGU general assembly 2021*. https://doi.org/10.5194/egusphere-egu21-16019

Engelund, F. (1970). Instability of erodible beds. *Journal of Fluid Mechanics*, *42*(2), 225–244. https://doi.org/10.1017/s0022112070001210

Engelund, F., & Fredsoe, J. (1982). Sediment ripples and dunes. *Annual Review of Fluid Mechanics*, *14*(1), 13–37. https://doi.org/10.1146/annurev.fl.14.010182.000305

Fernandez Luque, R., & Van Beek, R. (1976). Erosion and transport of bed-load sediment. *Journal of Hydraulic Research*, *14*(2), 127–144. https://doi.org/10.1080/00221687609499677

Fredsøe, J. (1974). On the development of dunes in erodible channels. *Journal of Fluid Mechanics*, *64*(1), 1–16. https://doi.org/10.1017/s0022112074001960

Fredsøe, J., & Deigaard, R. (1992). *Mechanics of coastal sediment transport* (Vol. 3). World Scientific.

Guy, H. P., Simons, D. B., & Richardson, E. V. (1966). *Summary of alluvial channel data from flume experiments, 1956-61*. US Government Printing Office.

Hersen, P., Andersen, K. H., Elbelrhiti, H., Andreotti, B., Claudin, P., & Douady, S. (2004). Corridors of barchan dunes: Stability and size selection. *Physical Review E*, *69*(1), 011304. https://doi.org/10.1103/physreve.69.011304

Jafarinik, S., Hernández Moreira, R., & Viparelli, E. (2019). Alluvial morphodynamics of bedrock reaches transporting mixed-size sand. Laboratory experiments. *Journal of Geophysical Research: Earth Surface*, *124*(12), 3067–3089. https://doi.org/10.1029/2019jf005058

Jafarinik, S., & Viparelli, E. (2020). Alluvial morphodynamics of low-slope bedrock reaches transporting nonuniform bed material. *Water Resources Research*, *56*(10), e2020WR027345. https://doi.org/10.1029/2020wr027345

Kennedy, J. F. (1969). The formation of sediment ripples, dunes, and antidunes. *Annual Review of Fluid Mechanics*, *1*(1), 147–168. https://doi.org/10.1146/annurev.fl.01.010169.001051

Khosronejad, A., & Sotiropoulos, F. (2017). On the Genesis and evolution of barchan dunes: Morphodynamics. *Journal of Fluid Mechanics*, *815*, 117–148. https://doi.org/10.1017/jfm.2016.880

Kleinhans, M., Wilbers, A., De Swaaf, A., & Van Den Berg, J. (2002). Sediment supply-limited bedforms in sand-gravel bed rivers. *Journal of Sedimentary Research*, *72*(5), 629–640. https://doi.org/10.1306/030702720629

Lesser, G. R., Roelvink, J. A., van Kester, J. A. T. M., & Stelling, G. S. (2004). Development and validation of a three-dimensional morphological model. *Coastal Engineering*, *51*(8–9), 883–915. https://doi.org/10.1016/j.coastaleng.2004.07.014

Parker, G., Klingeman, P. C., & McLean, D. G. (1982). Bedload and size distribution in paved gravel-bed streams. *Journal of the Hydraulics Division*, *108*(4), 544–571. https://doi.org/10.1061/jyceaj.0005854

Porcile, G., Blondeaux, P., & Colombini, M. (2020). Starved versus alluvial river bedforms: An experimental investigation. *Earth Surface Processes and Landforms*, *45*(5), 1229–1239. https://doi.org/10.1002/esp.4800

Porcile, G., Blondeaux, P., & Vittori, G. (2017). On the formation of periodic sandy mounds. *Continental Shelf Research*, *145*, 68–79. https://doi.org/10.1016/j.csr.2017.07.011

Reynolds, A. (1976). A decade's investigation of the stability of erodible stream beds. *Hydrology Research*, 7(3), 161–180. https://doi.org/10.2166/nh.1976.0012

Richards, K. J. (1980). The formation of ripples and dunes on an erodible bed. *Journal of Fluid Mechanics*, *99*(3), 597–618. https://doi.org/10.1017/s002211208000078x

Seminara, G. (2010). Fluvial sedimentary patterns. *Annual Review of Fluid Mechanics*, *42*(1), 43–66. https://doi.org/10.1146/annurev-fluid-121108-145612

Tuijnder, A. P., Ribberink, J. S., & Hulscher, S. J. (2009). An experimental study into the geometry of supply-limited dunes. *Sedimentology*, *56*(6), 1713–1727. https://doi.org/10.1111/j.1365-3091.2009.01054.x

Vanoni, V. A., & Brooks, N. H. (1957). *Laboratory studies of the roughness and suspended load of alluvial streams*. US Army Engineer Division.

Venditti, J. G., Nelson, P. A., Bradley, R. W., Haught, D., & Gitto, A. B. (2017). Bedforms, structures, patches, and sediment supply in gravel-bed rivers. In *Gravel-Bed Rivers: Process and Disasters*, (pp. 439–466).

Venditti, J. G., Nittrouer, J. A., Allison, M. A., Humphries, R. P., & Church, M. (2019). Supply-limited bedform patterns and scaling downstream of a gravel–sand transition. *Sedimentology*, *66*(6), 2538–2556. https://doi.org/10.1111/sed.12604

Worman, S. L., Murray, A. B., Littlewood, R., Andreotti, B., & Claudin, P. (2013). Modeling emergent large-scale structures of barchan dune fields. *Geology*, *41*(10), 1059–1062. https://doi.org/10.1130/g34482.1